JOURNAL OF GEOPHYSICAL RESEARCH, VOL. 110, B05S15, doi:10.1029/2004JB003356, 2005

# Onto what planes should Coulomb stress perturbations be resolved?

Sandy Steacy, Süleyman S. Nalbant, and John McCloskey
School of Environmental Sciences, University of Ulster, Coleraine, Northern Ireland, UK

Concetta Nostro
Istituto Nazionale di Geofisica e Vulcanologia, Rome, Italy

Oona Scotti and David Baumont
Institut de Radioprotection et de Sureté Nucléaire, Fontenay-aux-Roses, France

Received 31 July 2004; revised 21 March 2005; accepted 24 March 2005; published 7 May 2005.

[1] Coulomb stress maps are produced by computing the tensorial stress perturbation due to an earthquake rupture and resolving this tensor onto planes of a particular orientation. It is often assumed that aftershock fault planes are "optimally oriented"; in other words, the regional stress and coseismic stress change are used to compute the orientation of planes most likely to fail and the coseismic stress is resolved onto these orientations. This practice assumes that faults capable of sustaining aftershocks exist at all orientations, an assumption contradicted by the observation that aftershock focal mechanisms have strong preferred orientations consistent with mapped structural trends. Here we systematically investigate the best planes onto which stress should be resolved for the Landers, Hector Mine, Loma Prieta, and Northridge earthquakes by quantitatively comparing observed aftershock distributions with stress maps based on optimally oriented planes (two- and three-dimensional), main shock orientation, and regional structural trend. We find that the best model differs between different tectonic regions but that in all cases, models that incorporate the regional stress field tend to produce stress maps that best fit the observed aftershock distributions, although not all such models do so equally well. Our results suggest that when the regional stress field is poorly defined, or in structurally complex areas, the best model may be to fix the strike of the planes upon which the stress is to be resolved to that of the main shock but allow the dip and rake to vary.

**Citation:** Steacy, S., S. S. Nalbant, J. McCloskey, C. Nostro, O. Scotti, and D. Baumont (2005), Onto what planes should Coulomb stress perturbations be resolved?, *J. Geophys. Res.*, *110*, B05S15, doi:10.1029/2004JB003356.

## 1. Introduction

[2] It is now widely accepted that there is a causal relation between the static Coulomb stress perturbations resulting from earthquake slip and the triggering of subsequent events. This has been demonstrated for large earthquakes along both the North Anatolian [e.g., *Stein et al.*, 1997] and East Anatolian fault zones [*Nalbant et al.*, 2002], for moderate size events in southern California [*Harris et al.*, 1995], and for cascades of earthquakes of all scales, also in southern California [*Bak et al.*, 2002]. The relation is particularly strong for main shock–aftershock sequences where the pattern of Coulomb stress changes has been shown to affect the spatial distribution of aftershocks following a number of events, including the Loma Prieta [*Kilb et al.*, 1997], Landers [e.g., *Stein et al.*, 1992; *King et al.*, 1994], and Northridge [*Stein et al.*, 1994] earthquakes.


0148-0227/05/2004JB003356$09.00

[3] In the past few years, there has been a concerted research effort to move Coulomb stress analysis from a retrospective recognition of the influence of Coulomb stress to a practical tool that can be used to inform estimations of seismic hazard. This research has proceeded in two main directions: (1) modification of large earthquake probabilities based on a stress interaction term and generally involving a rate and state friction model [*Stein et al.*, 1997; *Toda et al.*, 1998; *Parsons et al.*, 2000] and (2) real-time assessment of the areas likely (and unlikely) to experience aftershocks [*McCloskey et al.*, 2003; *Steacy et al.*, 2004].

[4] Traditionally, stress tensors have either been resolved directly onto the planes of interest [e.g., *Harris and Simpson*, 1992; *Jaume and Sykes*, 1992; *Nalbant et al.*, 2002] or onto optimally oriented planes. The former is clearly best practice when the active structures are known, however, aftershocks frequently occur on unmapped structures and hence some assumptions must be made about the orientations of these. This is particularly important in the forward problem, where a "predictive" Coulomb stress map might look quite different depending on assumptions about the orientation of the active structures.

[5] In the now classic papers of *Stein et al.* [1992] and *King et al.* [1994], the authors resolved the stress perturbation tensor on to two-dimensional (2-D) optimally oriented planes, i.e., planes best oriented for failure in a strike-slip stress field containing both the regional stress and main shock induced stress perturbation tensors. In doing this, they explicitly assumed ''that planes optimally oriented for failure exist everywhere'', despite the tens of degrees rotation in predicted orientation observed near the causative fault plane. (This rotation explains why the main shock fault planes in their diagrams exhibit positive Coulomb stress). Regardless of questions about the physical nature of the optimally oriented planes assumption, in practice stress maps produced in this fashion have shown good qualitative agreement with aftershock distributions and this technique has been widely adopted by subsequent researchers [e.g., *King and Cocco*, 2001, and references therein].

[6] The optimally oriented planes assumption was challenged by *McCloskey et al.* [2003], who investigated the relation between aftershocks and fault structure. They observed a clear correlation between the orientations of mapped faults and both preshocks and aftershocks and suggested that stress maps could be constructed based on the structural information alone without the need to include the often poorly constrained regional stress field. Specifically, they recommended that stresses be resolved onto a suite of possible structures within the observed structural range and that the highest value of stress be selected at each point, in essence creating a worst-case map based on the orientation of the mapped structure. They presented an example of this for the Landers earthquake and showed that it qualitatively fit the observed aftershock distribution better than the stress map based on 2-D optimally oriented planes.

[7] Although stress maps based on both the 2-D optimally oriented planes assumption and the structurally based model have been shown to qualitatively correlate with spatial aftershock distributions, these models have not been quantitatively tested against each other nor have the best planes for resolving Coulomb stress been systematically (and quantitatively) investigated. If, however, Coulomb stress changes are to be computed within a few hours of main shock occurrence, we must know in advance how best to resolve the stress perturbation tensor. Here we investigate the best planes for resolving Coulomb stress for four California earthquakes (Figure 1). For each event, we consider 8–10 main models based on optimally oriented planes, main shock orientation, and structural trends, as well as a number of variations on each of these. We then quantitatively compare each stress map to the observed aftershock distribution. Note that in this study we assume a causal relation between Coulomb stress and aftershocks, the aim here is to determine how the choice of planes onto which the stress tensor is resolved affects the correlation between stress changes and the presence or absence of aftershocks, not to assess whether such a correlation exists.

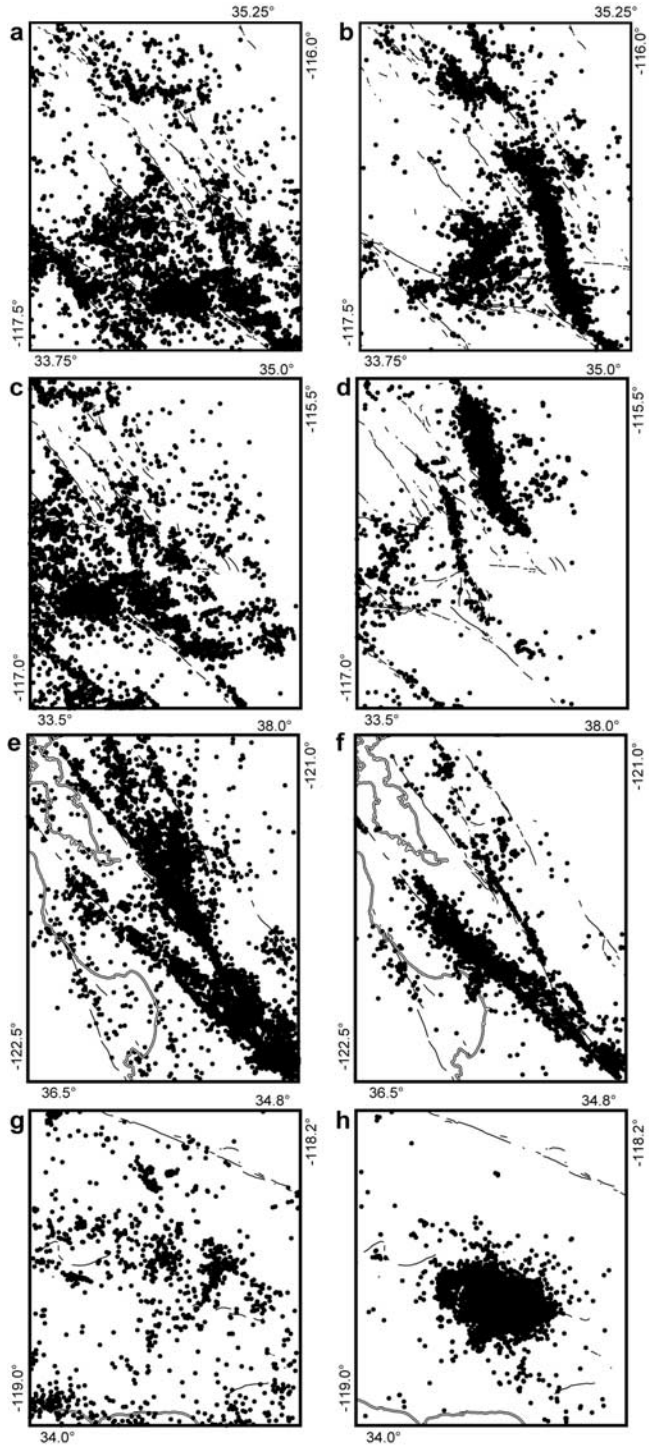


**Figure 1.** Regions of study and seismic activity used in the analysis. Temporal windows and number of events given in Table 2. (a) Landers preshocks, (b) Landers aftershocks, (c) Hector Mine preshocks, (d) Hector Mine aftershocks, (e) Loma Prieta preshocks, (f) Loma Prieta aftershocks, (g) Northridge preshocks, and (h) Northridge aftershocks.

## 2. Methodology

### 2.1. Main Shocks

[8] We select four California earthquakes for the analysis due to the ready availability of high-quality seismicity data, slip inversions, and structural data: the Loma Prieta, Land-

**Table 1.** Regional Stress Field Employed in Basic Models Described in Table 3

| Earthquake | Sigma 1, bars | Trend | Plunge | Sigma 2 | Trend | Plunge | Sigma 3 | Trend | Plunge |
|---|---|---|---|---|---|---|---|---|---|
| Landers | −100 | 7 | 0 | −10 | 0 | 90 | 0 | 97 | 0 |
| Hector Mine | −100 | 7 | 0 | −10 | 0 | 90 | 0 | 97 | 0 |
| Loma Prieta | −100 | 10 | 0 | −10 | 0 | 90 | 0 | 100 | 0 |
| Northridge | −100 | 16 | 0 | −10 | 106 | 0 | 0 | 0 | 90 |

ers, Hector Mine, and Northridge events. The Landers earthquake has become the gold standard of Coulomb research and here we investigate the Landers–Hector Mine sequence to test the robustness of our results over two strike-slip earthquakes closely related in time and space. We use the slip inversions of *Wald and Heaton* [1994] and *Ji et al.* [2002], respectively.

[9] The 1989 Loma Prieta earthquake was also primarily strike slip, although the slip inversion [*Wald et al.*, 1991] found a reverse component and a nonvertical fault plane with a dip of 70°. The region in which it occurred is known for mixed mode faulting with strike-slip and reverse faulting on near parallel structures [*Kovach and Beroza*, 1993]. The 1994 Northridge earthquake, by contrast, was a reverse faulting event on a plane dipping 40° [*Wald et al.*, 1996].

### 2.2. Coulomb Stress Calculations

[10] We calculate stress perturbation tensors and optimally oriented planes using the program "Farfalle" [*McCloskey et al.*, 2003]. This code allows us either to fix or allow to be free the orientation of each component of the planes of interest, hence we are able, for example, to compute the strike and rake of optimally oriented planes with a fixed dip. The program is also truly 3-D and thus the magnitude, trend, and plunge of each of the 3 principal axes of the regional stress must be specified. For comparison with earlier work we choose the average southern California orientation of the maximum principal stress as $\sigma_1$ = N7°E for the Landers and Hector Mine events [*Stein et al.*, 1992; *Hardebeck and Hauksson*, 2001], $\sigma_1$ = N16°E for the Northridge earthquake [*Stein et al.*, 1994], and $\sigma_1$ = N10°E for the Loma Prieta event, and assume that the magnitude of $\sigma_1 = -100$ bars (extension positive) in all cases [*Stein et al.*, 1992]. As the magnitudes of both the intermediate principal stress, $\sigma_2$, and the minimum principal stress, $\sigma_3$, are unconstrained, we arbitrarily set $\sigma_3 = 0$ [after *Stein et al.*, 1992] and initially choose a value of $\sigma_2$ = 10% $\sigma_1$, although we test the robustness of the results to this assumption (see below). As the Landers, Hector Mine, and Loma Prieta earthquakes occurred in primarily strike-slip tectonic regimes, in our analyses of these events we assume that $\sigma_2$ is the vertical stress; in the thrust regime of the Northridge earthquake we set $\sigma_2$ as a horizontal stress component and $\sigma_3$ as the vertical component (see Table 1).

[11] For each earthquake we define a spatial box (Table 2) around the event and compute the Coulomb stress perturbation on a regular grid for 10 (8 for Northridge) basic models. The calculation is performed on a horizontal planar grid at the intermediate depth of 7.5 km for the strike-slip regions (including Loma Prieta) and in 3-D for Northridge at every km depth between the surface and 15 km. Four of the models are variations of optimally oriented planes: 3-D optimally oriented planes with strike, dip, and rake free; 2-D optimally oriented planes with free strike but dip and rake fixed to the values of the main shock, and two 2.5-D models with either dip or rake fixed to the main shock value and other parameters free. We also consider two models based on the orientation of the main shock, one resolving the stress onto planes parallel to it with the same strike, dip, and rake; the other requiring planes to have the same strike as the main shock but allowing the dip and rake to vary based on the total stress field. We construct 2 similar models based on the mean structural orientation, with one using the regional structural trend to fix the dip and rake. Finally, we follow *McCloskey et al.* [2003] and resolve the stress tensor onto planes in a range of orientations consistent with the observed structure, in one case allowing only the strike to vary over some range, in the second allowing variation of the strike, dip, and rake. The naming convention for these models is given in Table 3.

[12] In addition to the 10 models described in Table 3, we also consider the sensitivity of the results to variations in the regional stress. For example, in the basic models we assume that $\sigma_2$ = 10% $\sigma_1$ as our experience has shown that in strike-slip regimes this value is generally large enough that the majority of 3-D optimally oriented planes have strike-slip mechanisms. In this sensitivity analysis we explore the effects of changing this relation to 5% $\sigma_1$ and 1% $\sigma_1$. We also consider possible errors in the orientation of $\sigma_1$, rotating it by ±10° and ±20° in conjunction with different magnitudes of $\sigma_2$. (Although greater rotations are possible, we felt that this range was reasonable given the error bars on stress orientations inferred from focal mechanisms [*Hardebeck and Hauksson*, 2001].) The naming convention for these different models is given in Table 4.

[13] Note that all calculations are performed using a value of the coefficient of friction of 0.7. This choice is based on a series of tests in which we ran the basic models for values of

**Table 2.** Spatial and Temporal Windows Used in Analysis[a]

| Earthquake | Date | Spatial Box[b] | Preshocks | Number of Preshocks | Aftershocks | Number of Aftershocks |
|---|---|---|---|---|---|---|
| Landers | 28 June 1992 | 33.75–35.25, −117.5 to −116. | 1 Jan. 1984 to 1 Jan. 1992 | 14444 | 28 June 1992 to 27 Dec. 1992 | 28658 |
| Hector Mine | 16 Oct. 1999 | 33.5–35, −117. to −115.5 | 1 Jan. 1984 to 1 Jan. 1992 | 15580 | 16 Oct. 1999 to 15 April 2000 | 12709 |
| Loma Prieta | 18 Oct. 1989 | 36.5–38, −122.5 to −121. | 1 Jan. 1979 to 17 Oct. 1989 | 41457 | 18 Oct. 1989 to 17 April 1990 | 10055 |
| Northridge | 17 Jan. 1994 | 34.–34.8, −119. to −118.2 | 1 Jan. 1984 to 16 Jan. 1994 | 1625 | 17 Jan. 1994 to 16 July 1994 | 8948 |

[a]Data sources are given in text.
[b]The first set of values is the latitude bounds, the second set is the longitude bounds.

**Table 3.** Naming Convention and Dependencies for 10 Basic Models[a]

| Model | Regional Stress? | Fixed Strike? | Fixed Dip? | Fixed Rake? |
|---|---|---|---|---|
| 3dop | y | n | n | n |
| 2dopdr | y | n | y, main shock | y, main shock |
| 2dopd | y | n | y, main shock | n |
| 2dopr | y | n | n | y, main shock |
| mains | y | y, main shock | n | n |
| strucs | y | y, structure | n | n |
| mainsdr | n | y, main shock | y, main shock | y, main shock |
| strucsdr | n | y, structure | y, structure | y, structure |
| res | n | n, structure $\pm 1/2$ SD | n, regular $\pm 20°$ | n, regular $\pm 45°$ |
| resdr | n | n, structure $\pm 1/2$ SD | y, structure | y, structure |

[a]Values of regional stress are given in Table 1, structural constraints are given in Table 5; abbreviations are y, yes; and n, no.

$\mu$ = 0.1, 0.2, ..., 0.9 and performed the statistical tests described in section 2.4. In most cases, and particularly for the optimally oriented planes, we observed very little difference between the different values of $\mu$; where differences were observed models with higher values tended to be better correlated with the aftershock distribution. This result is consistent with that obtained by *Steacy et al.* [2004] for 2-D optimally oriented planes.

### 2.3. Seismicity Data

[14] As discussed in section 2.4, we assess the success of each stress map in predicting the spatial distribution of aftershocks by computing the correlation coefficient between the two, following the methodology of *Steacy et al.* [2004], and compare the results to 2 null hypotheses based on the preshocks and a random earthquake distribution. In southern California, we use the relocated catalog from *Hauksson et al.* [2003] available from the Southern California Earthquake Center at http://www.data.scec.org/ftp/catalogs/hauksson/Socal_DD/, while in northern California we use the earthquake data from the Northern California Earthquake Data Center (http://quake.geo.berkeley.edu/). Note that we do not impose a cutoff magnitude but use all events within the space-time window of interest. As discussed in section 2.4, our statistical measure does not involve the computation of seismic rates and hence we choose to use all events available to us, rather than truncating the catalog at some magnitude of completeness.

[15] For each earthquake we create 2 catalogs: preshocks consisting of the seismicity in the area of interest prior to the event studied, and aftershocks occurring in the 6 months following the event. (Note that we select the short aftershock duration of 6 months for our study as recent work has shown that the contribution of the main shock to the overall stress perturbation decays rapidly with time [*Marsan*, 2003]). These windows and the number of events in each are given in Table 2 and the preshocks and aftershocks for each event are plotted in Figure 1.

### 2.4. Statistical Analysis

[16] *Steacy et al.* [2004] developed a simple technique to assess how well a given stress map "predicts" the spatial aftershock distribution that is based on computing the correlation coefficient between the two. Essentially, they gridded the stress map at a scale of about 1 km and at each grid point assigned the value of 1, 0, or −1 for positive, zero, or negative Coulomb stress. (In practice, few if any stress values equal 0). They then associated each seismic event with its nearest grid point and assigned the value 1 to each grid point containing one or more events, −1 for those containing no events. Finally, they computed the correlation coefficient between these two sets of values.

[17] This test is not designed to measure the correspondence between the magnitude of the Coulomb stress perturbation and seismicity rate changes but is, instead, a simple Boolean test to examine whether seismicity preferentially occurs in areas that experience positive Coulomb stress. The test implicitly assumes that all postmain shock seismicity is directly related to the Coulomb stress changes, hence in an ideal world all "aftershocks" would occur in areas experiencing positive Coulomb stress while there would be no seismicity in areas with negative stress changes. As stated earlier, we assume here that there is a causal relation between stress changes and the presence/absence of aftershocks, we are not testing this causality but are assessing the best technique for computing Coulomb stress maps.

[18] Note that even in this ideal world the actual value of the correlation coefficient might vary from main shock to main shock depending on the spatial coverage of both the stress changes and the aftershocks. The reason is that the measure contains a penalty for area so that, for instance, a stress map in which 50% of the area enjoyed positive stress and all aftershocks occurred in the positive stress regions would have a higher correlation coefficient than one with the same spatial distribution of aftershocks but in which 100% of the area experienced positive stress; the latter stress field would clearly have no predictive value. Moreover, as the preshock maps show, areas with high ambient seismicity rates might have experienced earthquakes during the aftershock period even in the absence of a perturbing main shock. While our correlation coefficient metric cannot distinguish these from truly triggered aftershocks, we attempt to account for this in how we assess the significance of measured coefficients.

[19] We assess the significance of the value of the correlation coefficient by comparing it with values computed for two null hypotheses, a purely random spatial distribution of seismicity and the seismicity preceding the main shock of interest. Only if the correlation coefficient between the stress field and the aftershocks is greater than that between the stress field and both of the two null cases, do we consider that the stress map has any predictive value. To gauge the robustness of the computed correlation coefficients we

**Table 4.** Naming Convention for Sensitivity Models[a]

| Model | Sigma 1 Rotation | Vertical Stress |
|---|---|---|
| p10 | 10° clockwise | 10% sigma 1 |
| p20 | 20° clockwise | 10% sigma 1 |
| m10 | 10° counterclockwise | 10% sigma 1 |
| m20 | 20° counterclockwise | 10% sigma 1 |
| 5 | as named above | 5% sigma 1 |
| 1 | as named above | 1% sigma 1 |

[a]Note that multiple names can be used; hence 3dop5p10 indicates a 3-D optimally oriented planes model with a clockwise rotation of $\sigma_1$ by 10° with respect to the orientation listed in Table 1 and a magnitude of $\sigma_2$ of 5% $\sigma_1$.

randomly sample 10 subsets of each data set and compute the mean and standard deviation.

[20] The null hypotheses correspond to progressively more refined knowledge of the seismicity in the main shock region. While a purely random spatial distribution of seismicity is clearly oversimplified, because the test is Boolean and hence one or more events at the same location counts as one, this test will give the same results as one with more clustered seismicity provided that the relative proportion of filled/unfilled grid nodes remains the same. In the second null hypothesis, preshocks are assumed to "illuminate" many of the same fault structures that experience aftershocks. Hence, if the value of the correlation coefficient between the stress map and the aftershocks is greater than the value between the stress and the preshocks, then this implies that the Coulomb stress map is delineating areas where seismicity has been enhanced (positive stress) or suppressed (negative).

[21] Note that we first exclude all grid points and seismicity data occurring within 5 km of the fault used in the stress computation. Our primary reason for this is that as discussed in section 2.2, optimally oriented planes models generally show positive stress along the causative fault plane and, hence, since most aftershocks occur near the fault plane, will tend to do statistically better than models with near-fault relaxation. From a seismic hazard perspective, however, we are interested in off-fault aftershocks (since we already know that aftershocks will occur along the fault zone) and therefore we wish to distinguish between the ability of the different models to identify the off-fault regions where these aftershocks are likely to occur.

## 3. Results

[22] *McCloskey et al.* [2003] developed a graphical technique to compare the orientations of fault structures to the observed focal mechanisms in the same area, and applied it in California. For each fault in the digital California fault map [*California Department of Conservation*, 2000] in the region of interest, they computed the orientation of each 1 km segment along the structure and plotted a rose diagram of the binned results with orientations flipped by 180° if necessary so that all faults plotted in the same hemisphere. They then plotted the orientations of the focal mechanism nodal planes in the same fashion, where they chose the nodal plane most closely aligned with the regional structural trend, and computed the vector means and standard deviations of the two distributions.

[23] Figure 2 shows the results of the structural analyses using this technique for each earthquake region in the current study. For each event we include two plots, the first compares the regional structural trend with the orientation of the preshock nodal planes most closely aligned with the regional structural trend, the second the same fault structure compared to the aftershock nodal planes. In all cases, only events with magnitude >3.5 are shown.

[24] The results for the Landers area are given in Figure 2a. As Figure 2a (left) illustrates, the pre-Landers seismicity occurs on planes with a mean orientation almost identical to that of the mapped structure, 322° and 326°, respectively. The aftershocks have a similar mean orientation, 329°, although a small number of thrust events with a more E-W orientation are also observed.

[25] As illustrated in Figure 2b, the Hector Mine region shows a slight structural rotation compared to Landers, with a structural mean of 328° and a preshock mean orientation of 320°. The aftershock distribution also contains relatively more thrust events (the E-W planes in Figure 2b), and this is reflected in the standard deviation of the distribution (Table 5).

[26] The Loma Prieta earthquake occurred in an area of nearly uniformly oriented structure and this is clearly seen both in Figure 2c and in the standard deviation given in Table 5. The aftershock focal mechanisms, by contrast, while predominantly strike slip, include a moderate percentage of thrust events. Finally, and unsurprisingly, the Northridge aftershock distribution (Figure 2d) is composed mainly of thrust events consistent with the fault structure in that region.

[27] The results from this structural analysis are tabulated in Table 5 and are used to construct four of the basic models: one in which the strike of the planes upon which stress is resolved is fixed to the value of the mean regional structural trend, another where strike is similarly fixed, as is dip and rake based on the observed strike-slip trend (i.e., dip 90°, rake 180°), a third in which stress is resolved onto planes with a range of orientations defined from $-1/2$ to $+1/2$ of standard deviation of the mean orientation, dip and rake are also allowed to vary, and the plane with the largest stress is chosen; and finally, one where the strike is allowed to vary as above but the dip and rake are fixed.. (In other words, we calculate stresses on a series of planes with strikes at 1° intervals within these ranges (316.1° to 335.5° for the Landers earthquake, see Table 5) and choose the largest Coulomb stress value.)

### 3.1. Basic Models

[28] Stress maps are shown in Figure 3 for the Landers stress perturbation resolved onto the 10 basic models described in Table 3. In each map we also show the predicted (or prescribed) focal mechanism as this aids in understanding the reasons for the different stress patterns. Note that for the optimally oriented planes models, the focal mechanisms were constructed by choosing the nodal plane

**Figure 2.** Comparison of structural and seismicity orientation for the regions surrounding the (a) Landers, (b) Hector Mine, (c) Loma Prieta, and (d) Northridge earthquake. (left) Fault structure (top for all events except on left for Northridge) and the orientation of the preshock nodal planes most closely aligned with the regional structural trend (lower half of each plot, except for Northridge, which is the right half). (right) Comparison of same structural trend with the aftershock orientations. In all cases, the temporal and spatial windows are the same as given in Table 2, although only earthquakes with $M > 3.5$ are included here and data sources differ. Southern California focal mechanisms are from *Hauksson* [2000] (http://www.data.scec.org/ftp/catalogs/hauksson/Socal_focal), and Northern California data are from Northern California Earthquake Data Center (http://quake.geo.berkeley.edu/).

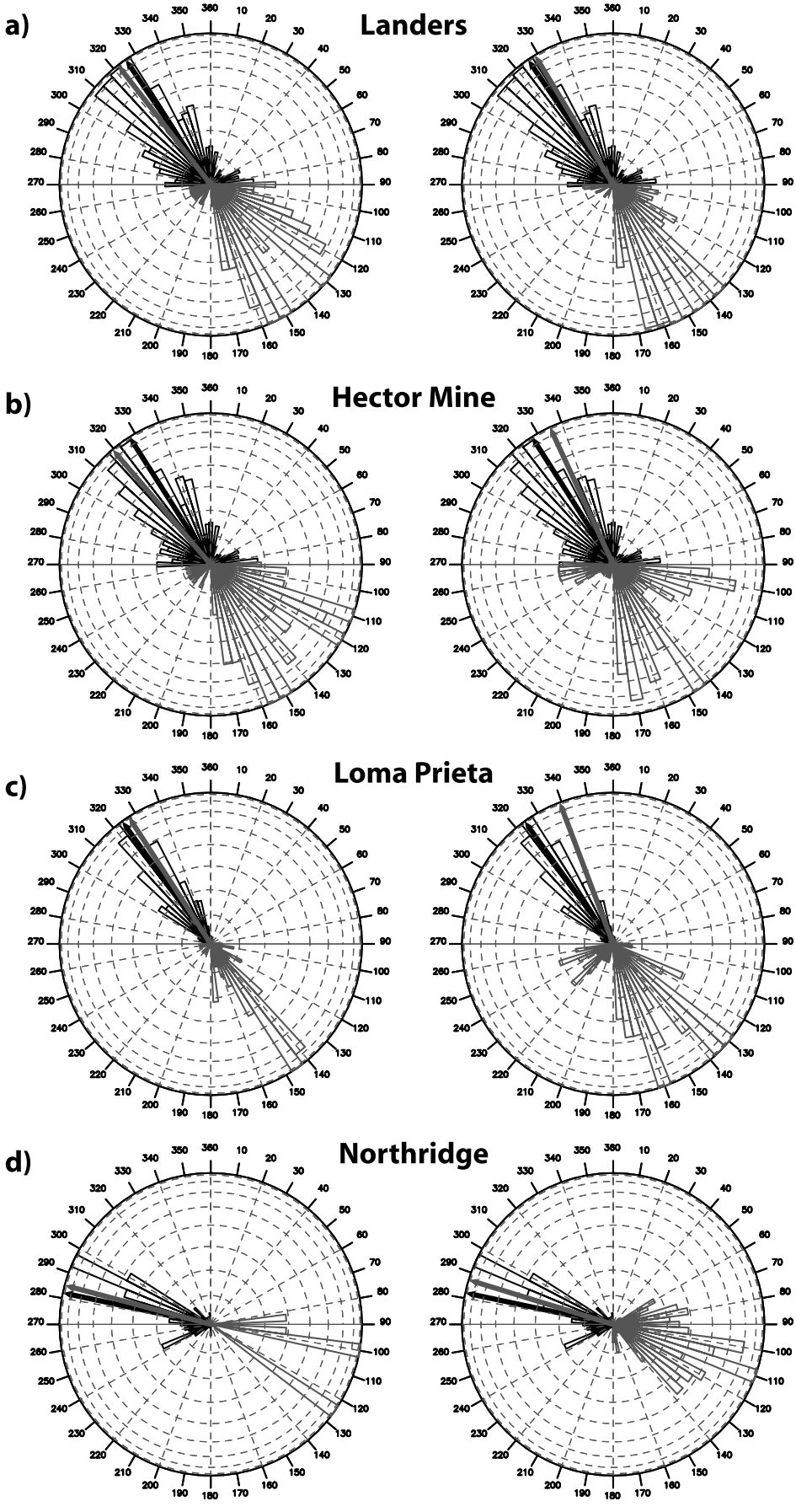


**Figure 2**

**Table 5.** Results for the Analysis Shown in Figure 2[a]

| Earthquake | Earthquake Strike | Structure | | Preshock | | Aftershock | |
|---|---|---|---|---|---|---|---|
| | | Mean | SD | Mean | SD | Mean | SD |
| Landers | 355 | 325.7 | 19.6 | 322.1 | 18.1 | 328.5 | 15.9 |
| Hector Mine | 343 | 327.5 | 20.1 | 319.5 | 17.3 | 330.62 | 24.8 |
| Loma Prieta | 308 | 324.1 | 9 | 327.1 | 14.8 | 340.9 | 19.5 |
| Northridge | 302 | 282 | 13.7 | 284.9 | 7.5 | 286.3 | 13.1 |

[a]Values for the fault structure are used in construction of the models strucs, strucsdr, res, and resdr.

most consistent with the regional structure and computing its conjugate, hence only one nodal plane corresponds to the orientation of one of the optimally oriented planes.

[29] As Figure 3 shows, the models have a number of similarities, particularly the large positive lobe to the SW (the area of the large Big Bear aftershock) as well as positive stress regions at the fault ends and to the NE, but there are also a number of striking differences between both the stress maps and the predicted focal mechanisms.

[30] Figures 3a–3d, for optimally oriented planes, are superficially similar although 2a (3-D optimally oriented planes) has a larger positive lobe surrounding the northern portion of the fault and it predicts thrust events in the vicinity of the fault planes. The width of the positive area along the fault traces increases for the three 2-D optimally oriented planes models from quite narrow (fixed dip and rake), to slightly wider (fixed dip) with some predicted oblique slip mechanisms, to almost as wide as the 3-D case (free dip but fixed rake) with more predicted oblique slip mechanisms close to the fault plane.

[31] The maps for the models based on main shock and structural orientations but also including the influence of the regional stress field are shown in Figures 3e and 3f. The stress field in Figure 3e based on main shock orientation but free dip and rake is qualitatively similar to that of the 2-D optimally oriented planes model with fixed rake (Figure 3d), although the orientation of these predicted planes differs because it is fixed in Figure 3e and allowed to vary in Figure 3d. By contrast, the model based on the orientation of the structure predicts oblique slip focal mechanisms throughout the region. (Note that in both models one nodal plane is parallel to the fixed strike but this can be difficult to see in some of the near-fault focal mechanisms in Figure 3e due to the extremely shallow dip predicted at these locations).

[32] The variations on these models in which strike, dip, and rake are fixed are shown in Figures 3g and 3h. These models are superficially similar to Figure 3b but in each case the stress field is slightly rotated with respect to this model. Finally, Figures 3i and 3j show the stress fields for the models in which stress is resolved on a range of possible orientations and the orientation experiencing is highest stress is selected. Not surprisingly, a higher proportion of the total area experiences positive Coulomb stress than for the other models. Additionally, in the model in which the dip and rake are also allowed to vary (Figure 3j), the

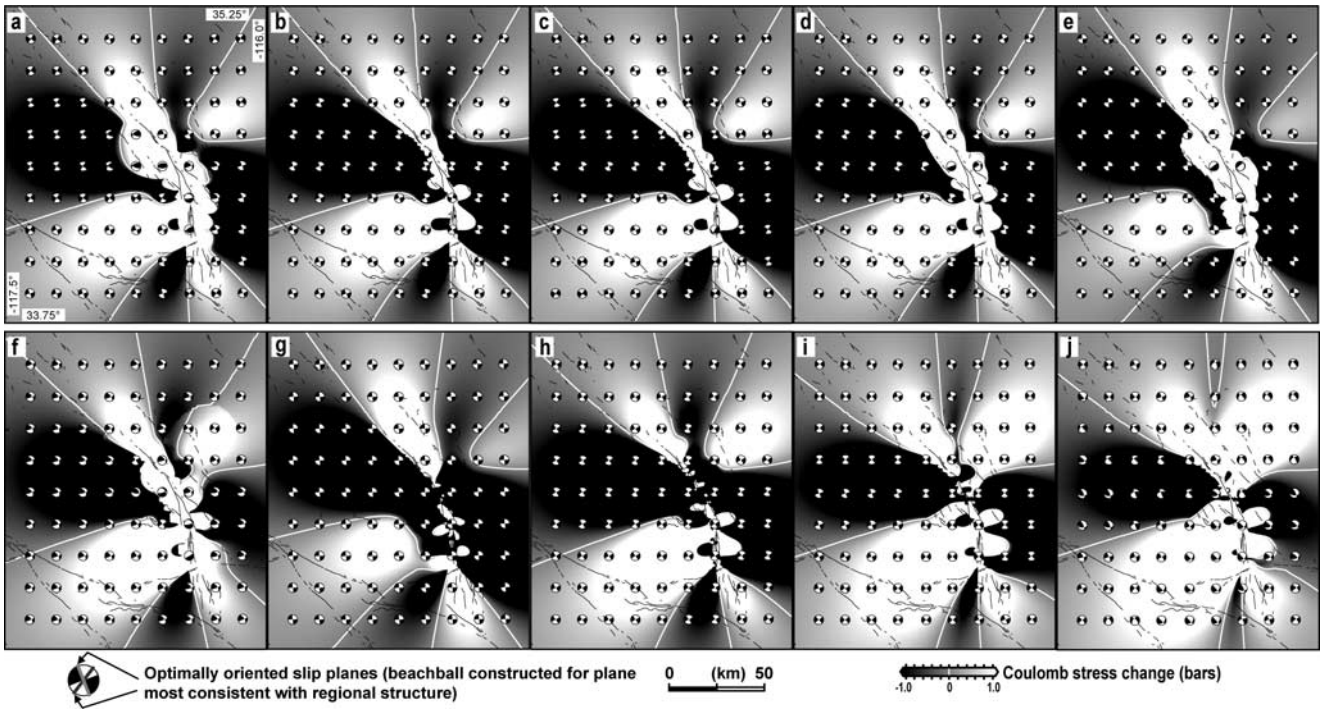


**Figure 3.** Stress fields and predicted focal mechanisms produced by 10 basic Landers models for (a) 3-D optimally oriented planes, (b) 2-D optimally oriented planes with fixed dip and rake, (c) 2-D optimally oriented planes with fixed dip, (d) 2-D optimally oriented planes with fixed rake, (e) fixed strike from main shock orientation but free dip and rake, (f) fixed strike from structural orientation but free dip and rake, (g) fixed strike, dip, and rake based on main shock orientation, (h) fixed strike, dip, and rake based on structural orientation, (i) varying strike within a range defined by the structural trend, and (j) varying strike, dip, and rake within a range defined by the structural trend.

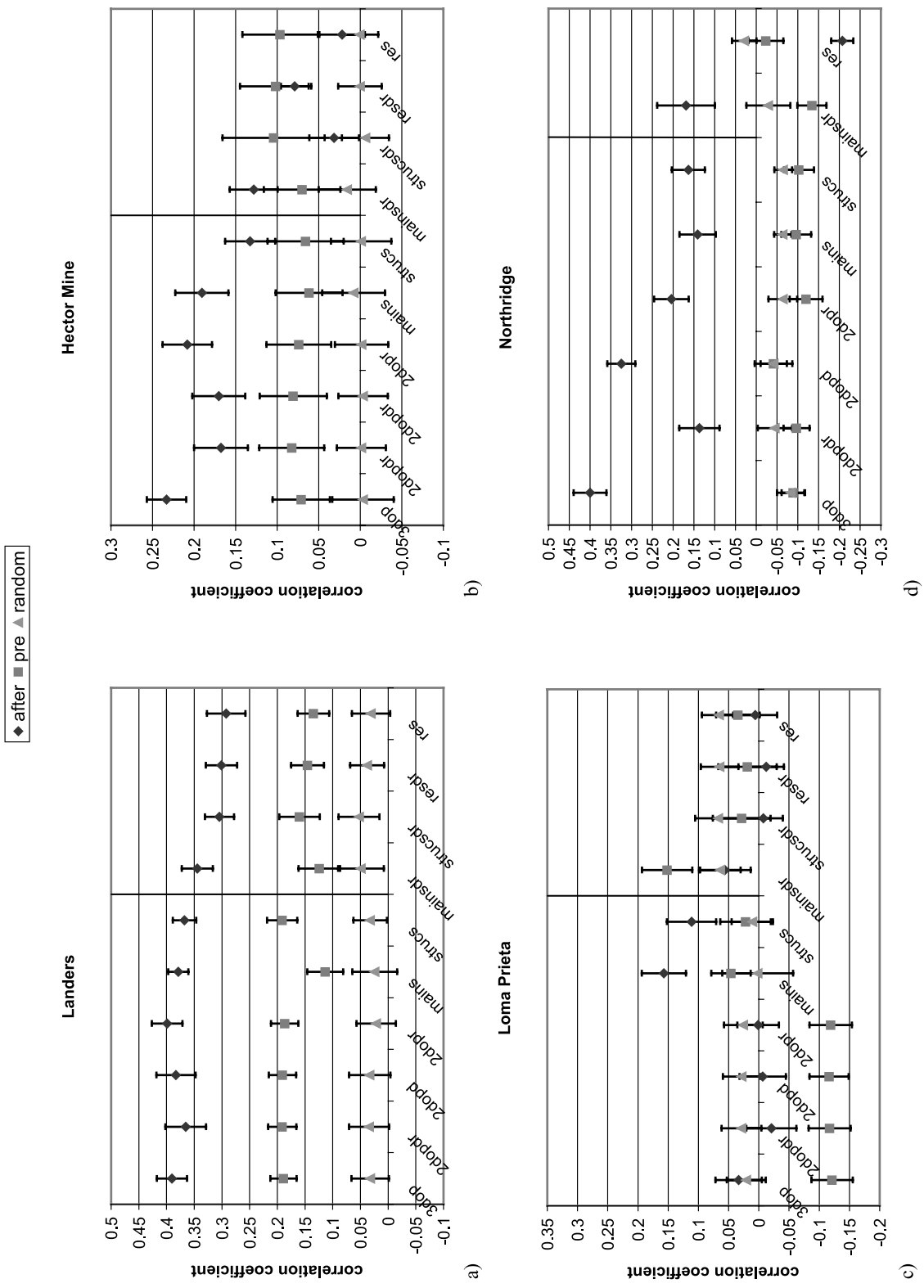
◆ after ■ pre ▲ random
Landers
Hector Mine
Loma Prieta
Northridge
correlation coefficient
a)
b)
c)
d)
3dop
2dopdr
2dopd
2dopr
mains
strucs
mainsdr
strucsdr
resdr
res

**Figure 4**

predicted focal mechanisms tend to be oblique slip with a significant thrust component.

[33] The results for the basic models are shown in Figure 4. As Figure 4a shows, there is a high correspondence between the Landers stress maps and its aftershock distribution for all the models, and this correlation is higher for the aftershock distribution than for either of the two null hypotheses. The six models involving the regional stress field exhibit the highest correlation coefficients, although a stress map based purely on the main shock orientation (strike, dip, and rake) has equivalent values within error.

[34] The results for the Hector Mine earthquake are shown in Figure 4b. Unlike the Landers earthquake, here we observe that the only models with greater correlation coefficients than the null hypotheses are optimally oriented planes and the model based on the main shock orientation but with free strike and dip. Note as well that the scales are different and that the values of the correlation coefficients for the Hector Mine earthquake are lower than those for the Landers event. This results from the penalty for area described in section 2.4; because the Landers aftershocks fill the positive stress lobes to a greater extent than do the Hector Mine aftershocks, the correlation coefficients are higher.

[35] Figure 4c shows that in the region of complex faulting around the Loma Prieta earthquake, only the models based on main shock and structural orientation with freely varying dip and rake have higher correlation coefficients than the null hypotheses. Finally, in Figure 4d we observe that for the Northridge earthquake all the models, with the exception of the one in which stress is resolved onto a range of structural orientations with varying dip and rake, have higher correlation coefficients than the null hypotheses, and the 3-D optimally oriented planes and 2-D optimally oriented planes with fixed dip have the highest values. The latter is perhaps surprising but arises from the fact that there is little qualitative difference in either the stress field or the predicted focal mechanisms of the two, at least in a slice of the 2 models.

### 3.2. Sensitivity to Regional Stress

[36] The sensitivity of the results in Figure 4 to variations in the regional stress field is shown in Figures 5–7. In Figure 5, we examine the effect on the 3-D optimally oriented planes models of horizontal rotations in the orientation of the principal component of stress $\sigma_1$ and of changing the magnitude of the intermediate component of stress $\sigma_2$. As Figure 5a shows, the correlation coefficients computed for the Landers earthquake are fairly robust to horizontal rotation but markedly decrease when $\sigma_2$ is decreased. By contrast, the Hector Mine results (Figure 5b) are much more sensitive to the orientation of $\sigma_1$ (with correlation coefficients less than the null hypotheses for counterclockwise stress rotation of 20°) but do not change within error as the magnitude of $\sigma_2$ is reduced.

[37] The results for the Loma Prieta earthquake (Figure 5c) show that the correlation coefficient increases to values greater than the null hypotheses for a clockwise stress rotation of 20° and no change in the magnitude of $\sigma_2$ and for all but one model when $\sigma_2$ is reduced to 1% of $\sigma_1$. As Figure 5d illustrates, the Northridge results are robust to all the variations examined here.

[38] The effect of horizontal rotation of $\sigma_1$ and reduction of the magnitude of $\sigma_2$ on 2-D optimally oriented planes is shown in Figure 6. The results here are for the model with fixed rake but freely varying strike and dip; similar results are observed for the other models with 2-D optimally oriented planes. For the Landers and Hector Mine earthquakes (Figures 6a and 6b), the effects of varying the orientation of $\sigma_1$ are very similar to those for the 3-D optimally oriented planes models (Figures 5a and 5b), although in the 2-D case the reduction of $\sigma_2$ leaves the correlation coefficient unchanged. The results for the Loma Prieta earthquake (Figure 6c) are also similar to the 3-D results, again the correlation coefficient increases to a value greater than the null hypotheses only for a clockwise stress rotation of 20° while, as in Figures 6a and 6b, reduction of $\sigma_2$ leaves the results unchanged. As in the 3-D case, varying the regional stress field for the Northridge earthquake has no effect on the results (Figure 6d).

[39] Figure 7 shows the sensitivity to variations in the regional stress of the model in which strike is fixed to that of the main shock but dip and rake are allowed to vary. In general, the Landers, Hector Mine, and Northridge results (Figures 7a, 7b, and 7d, respectively) show little change with respect to either rotations in the orientation of $\sigma_1$ or changes in the magnitude of $\sigma_2$, with the exception of the Landers case with a counterclockwise stress rotation of 20°. The values of the correlation coefficient for Northridge, however, are much lower than for 3-D optimally oriented planes although still greater than those for the null hypotheses. For the Loma Prieta earthquake, this model and the one based on structural orientation are the only ones to exhibit greater correlation coefficients than the null hypotheses; both models have slightly higher values of the statistic with clockwise rotation of $\sigma_1$, lesser values with

**Figure 4.** Results for the 10 basic models for the four main shocks in this study: (a) Landers, (b) Hector Mine, (c) Loma Prieta, and (d) Northridge earthquakes. In this and Figures 5–7 we plot the correlation coefficient between each stress map and three sets of data: aftershocks (diamonds), preshocks (squares), and randomly located events (triangles). Each point represents the mean correlation coefficient of 10 randomly sampled subsets of the data and the error bars indicate the standard deviation. In Figures 4a–4c the six models to the left of the vertical line are those that depend in some way on the regional stress field: from left to right, 3-D optimally oriented planes, 2-D optimally oriented planes with fixed dip and rake, 2-D optimally oriented planes with fixed dip, 2-D optimally oriented planes with fixed rake, fixed strike based on the main shock but free dip and rake, and fixed strike based on the regional structural trend but free dip and rake. The models to the right of the vertical line are independent of the regional stress field: fixed strike, dip, and rake based on the main shock, fixed strike, dip, and rake based on the structure, a range of strikes based on the structure but with fixed dip and rake, and a range of strikes, dips, and rakes based on the structure. In the Northridge case, the models that require information about the dip of the regional structure are omitted.

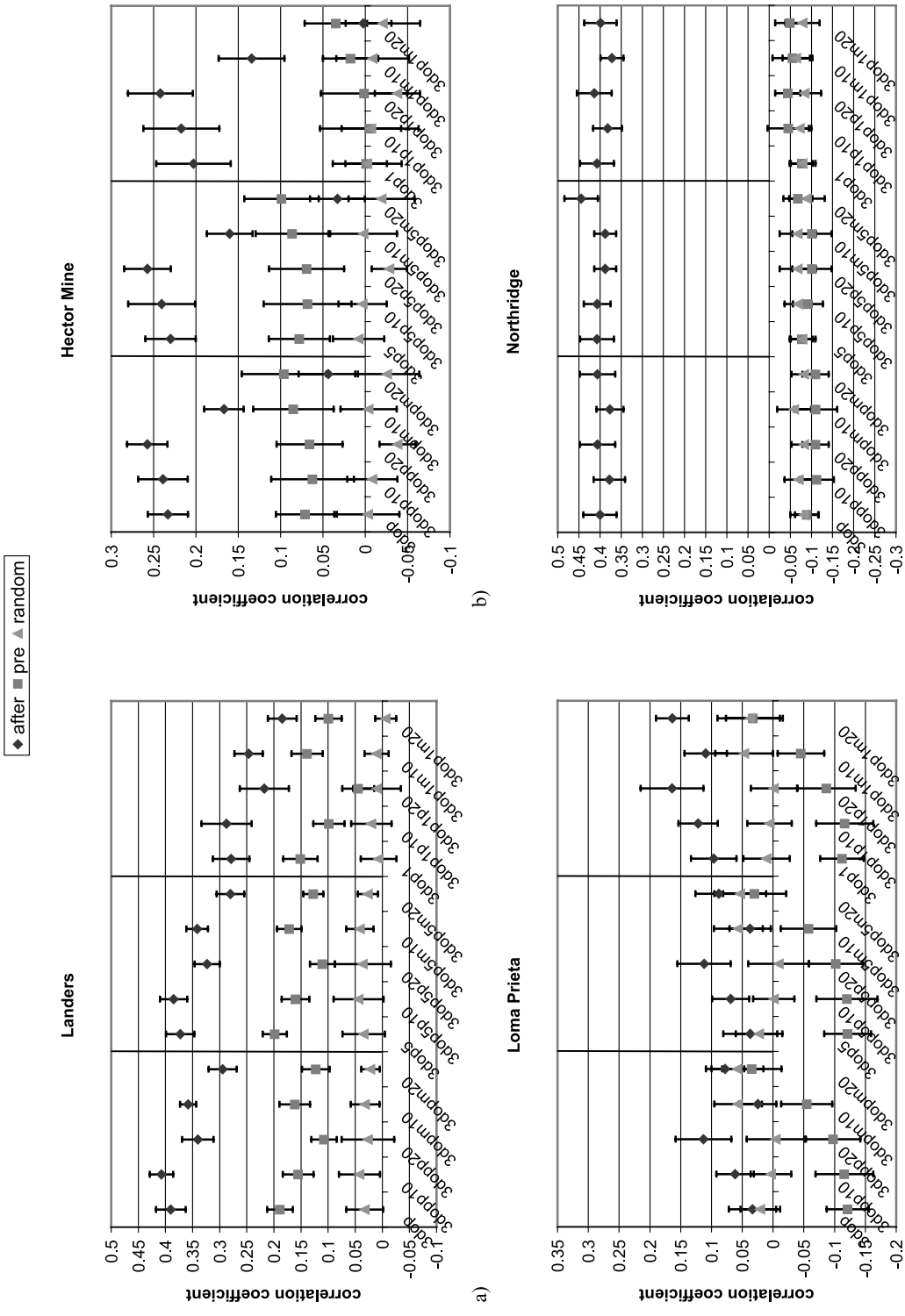


**Figure 5.** Effect of varying the regional stress field on the correlation coefficient for 3-D optimally oriented planes models for (a) Landers, (b) Hector Mine, (c) Loma Prieta, and (d) Northridge earthquakes. Vertical lines separate models with different values of the vertical stress. The first set of results is for the basic 3-D optimally oriented planes model (i.e., this point is the same as the first point in each diagram in Figure 4), this model with a 10° clockwise rotation of the horizontal stress field, with a 20° clockwise rotation, a 10° counterclockwise rotation, and a 20° counterclockwise rotation. The next set repeats these except that $\sigma_2 = 5\%\ \sigma_1$ and in the final set, $\sigma_2 = 1\%\ \sigma_1$.

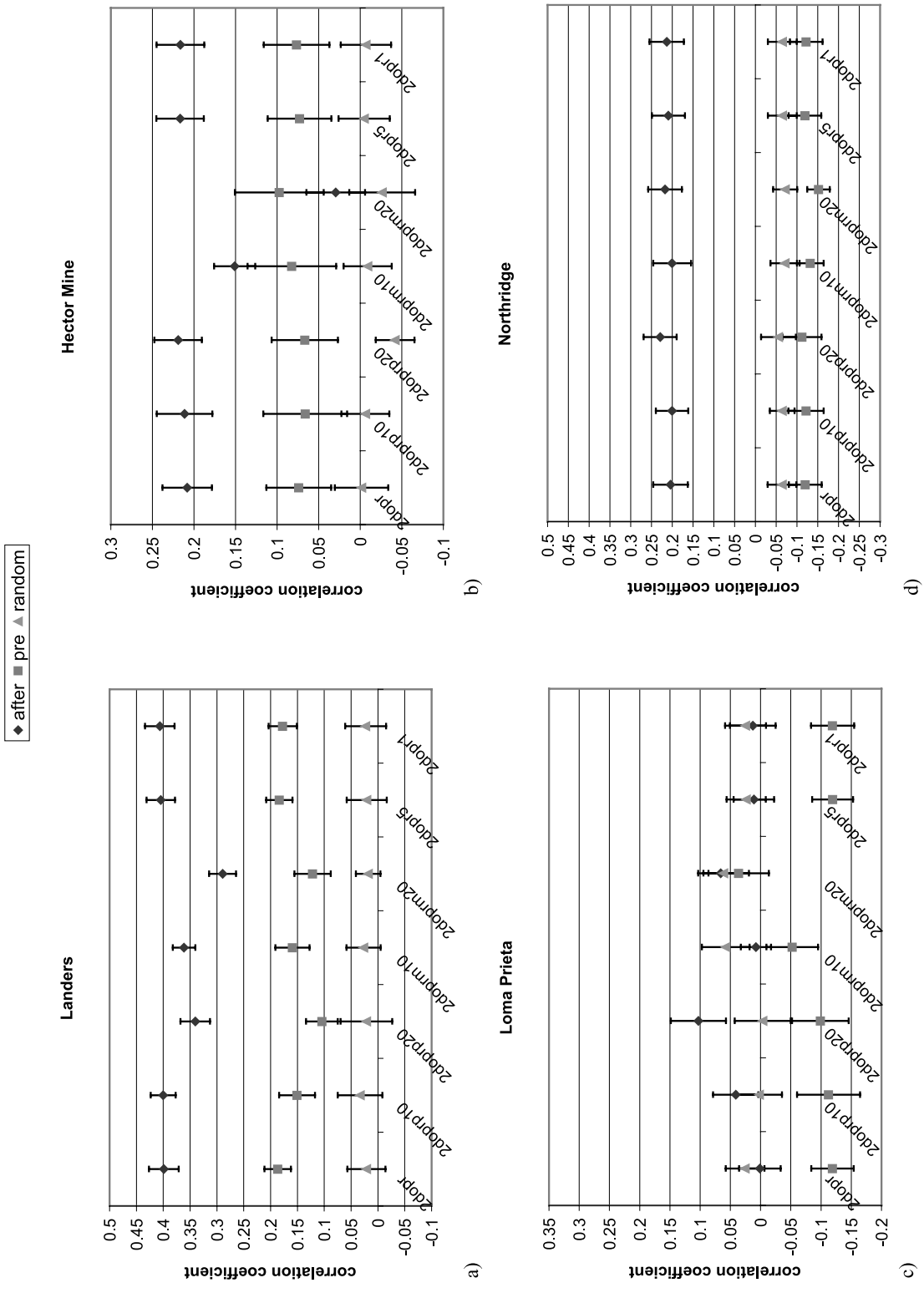


**Figure 6.** Effect of varying the regional stress field on the correlation coefficient for 2-D optimally oriented planes model with fixed rake for (a) Landers, (b) Hector Mine, (c) Loma Prieta, and (d) Northridge earthquakes. The first set of results is for the basic 2-D optimally oriented planes model with fixed rake (i.e., this point is the same as the fourth point in each diagram in Figure 4), this model with a 10° clockwise rotation of the horizontal stress field, with a 20° clockwise rotation, a 10° counterclockwise rotation, a 20° counterclockwise rotation, a reduction in $\sigma_2$ to 5% $\sigma_1$, and a reduction in $\sigma_2$ to 1% $\sigma_1$.

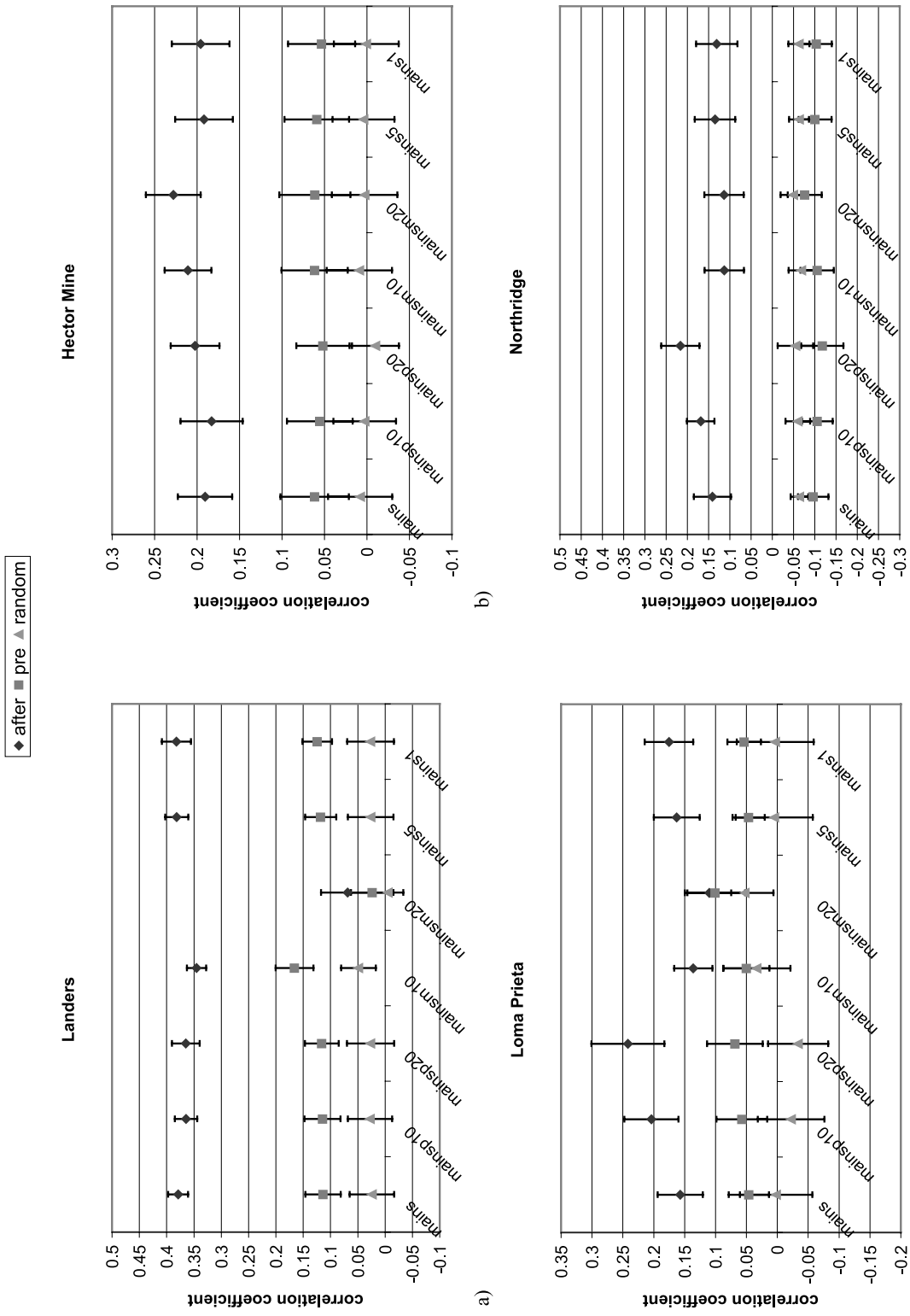


**Figure 7.** Effect of varying the regional stress field on the correlation coefficient for model in which strike is fixed to that of the main shock but dip and rake are allowed to vary for (a) Landers, (b) Hector Mine, (c) Loma Prieta, and (d) Northridge. The first set of results is for basic mains model (i.e., this point is the same as the fifth point in each diagram in Figure 4), this model with a 10° clockwise rotation of the horizontal stress field, with a 20° clockwise rotation, a 10° counterclockwise rotation, a 20° counterclockwise rotation, a reduction in $\sigma_2$ to 5% $\sigma_1$, and a reduction in $\sigma_2$ to 1% $\sigma_1$.

counter clockwise rotation, and little sensitivity to the magnitude of $\sigma_2$.

## 4. Discussion

[40] The aim of this paper is to assess the planes upon which Coulomb stress should be resolved in order to achieve the greatest correspondence between stress changes and aftershock locations immediately following the occurrence of a moderate to large earthquake. As the results show, in simple, predominantly strike-slip or thrust environments, the greatest correspondence between stress maps and the spatial aftershock distributions is observed when stress is resolved onto 3-D optimally oriented planes.

[41] This correspondence is sensitive to the regional stress field, however, and in strike-slip regions it particularly depends on the magnitude of the vertical component of stress, $\sigma_2$. When the vertical stress is low, the predicted optimally oriented planes often have thrust mechanisms whereas a higher vertical stress component leads to predominantly strike-slip mechanisms. Hence the values of the correlation coefficient for the 3-D optimally oriented planes when the vertical stress is reduced to 1% of the principal horizontal stress decreases by about 25% for the Landers results (Figure 5a) but only decreases by about 10% for the Hector Mine case (Figure 5b) where more thrust aftershocks are observed (Figure 2b). In the mixed mode faulting environment in which the Loma Prieta earthquake occurred, the correlation coefficient increases when the vertical stress is reduced.

[42] The results for 2-D optimally oriented planes, by contrast, show little sensitivity to the magnitude of the vertical component of stress and hence may be a better choice in predominantly strike-slip regions. These results are, however, sensitive to horizontal rotations in the orientation of the principal component of stress. The results for models based on the orientation of the main shock but with freely varying strike and dip are generally less sensitive to changes in regional stress and might be more appropriate when the regional stress field is not well constrained.

[43] In practice, of course, the models discussed in this paper would be used as starting points and might be expected to be modified as an aftershock sequence developed. So, for example, following an earthquake in a thrust faulting region, a researcher might initially choose to resolve stresses on to 3-D optimally oriented planes using the best constrained regional stress field available, then modify this field to improve the correspondence between stress changes and seismicity.

## 5. Conclusions

[44] 1. In the regions surrounding the four earthquakes in this study, there is a clear correspondence between the orientation of the mapped structure and both the premain shock and postmain shock seismicity.

[45] 2. The planes upon which Coulomb stress should be resolved in order to achieve the greatest correspondence between positive stress and aftershock location varies between the different tectonic regions investigated.

[46] 3. In all cases, models that incorporate the regional stress field have a greater predictive capacity (i.e., produce stress maps that are more highly correlated with the observed spatial aftershock distribution) than those that do not.

[47] 4. The 3-D models are particularly sensitive to the magnitude of $\sigma_2$ when it is the vertical stress with low values encouraging reverse or oblique slip focal mechanisms and higher values discouraging them. Therefore the magnitude of this parameter should be chosen with care to produce stress fields consistent with the fault structure in the region of interest.

[48] 5. The 2-D models are sensitive to the orientation of the principal horizontal stress and a rotation of 20° can make the difference between a map that correlates well with the aftershock distribution and one that does not.

[49] 6. In areas where the regional stress is poorly defined, or the structure complex, a starting model in which planes are assumed to be parallel to the main shock orientation but dip and rake are allowed to vary may lead to production of a stress map that correlates well with the aftershock distribution.

[50] **Acknowledgments.** We thank the Associate Editor Joan Gomberg and Shinji Toda for detailed and constructive reviews that greatly improved the manuscript. This work was supported by the UK Natural Environment Research Council (GR8/04407) and the European Commission under Framework 5 (PRESAP, EVG1-CT-1999-0001).

## References

Bak, P., K. Christensen, L. Danon, and T. Scanlon (2002), Unified scaling law for earthquakes, *Phys. Rev. Lett.*, doi:10.1103/PhysRevLett.88.178501.

California Department of Conservation (2000), Digital database of faults from the fault activity map of California and adjacent areas, *Publ. CD 2000-006*, Div. of Mines and Geol., Sacramento.

Hardebeck, J., and E. Hauksson (2001), Crustal stress field in southern California and its implications for fault mechanics, *J. Geophys. Res.*, *106*, 21,859–21,882.

Harris, R. A., and R. W. Simpson (1992), Changes in static stress on the southern California faults after the 1992 Landers earthquake, *Nature*, *360*, 251–254.

Harris, R. A., R. W. Simpson, and P. A. Reasenberg (1995), Influence of static stress changes on earthquake locations in southern California, *Nature*, *375*, 221–224.

Hauksson, E. (2000), Crustal structure and seismicity distribution adjacent to the Pacific and North America plate boundary in southern California, *J. Geophys. Res.*, *105*, 13,875–13,903.

Hauksson, E., W.-C. Chi, and P. Shearer (2003), Comprehensive waveform cross-correlation of southern California seismograms: part 1. Refined hypocenters obtained using the double-difference method and tectonic implications, *Eos Trans. AGU*, *84*(46), Fall Meet. Suppl., Abstract S21D-0325.

Jaume, S. C., and L. R. Sykes (1992), Changes in state of stress on the southern San Andreas fault resulting from the California earthquake sequence of April to June 1992, *Science*, *258*, 1325–1328.

Ji, C., D. J. Wald, and D. V. Helmberger (2002), Source description of the 1999 Hector Mine, California, earthquake, part II: Complexity of slip history, *Bull. Seismol. Soc. Am.*, *92*(4), 1208–1226.

Kilb, D., M. Ellis, J. Gomberg, and S. Davis (1997), On the origin of diverse aftershock mechanisms following the 1989 Loma Prieta earthquake, *Geophys. J. Int.*, *128*, 557–570.

King, G. C. P., and M. Cocco (2001), Fault interaction by elastic stress changes: New clues from earthquake sequences, *Adv. Geophys.*, *44*, 1–38.

King, G. C. P., R. S. Stein, and J. Lin (1994), Static stress changes and the triggering of earthquakes, *Bull. Seismol. Soc. Am.*, *84*, 935–953.

Kovach, R. L., and G. Beroza (1993), Seismic potential from reverse faulting on the San Francisco Peninsula, *Bull. Seismol. Soc. Am.*, *83*, 597–602.

Marsan, D. (2003), Triggering of seismicity at short timescales following Californian earthquakes, *J. Geophys. Res.*, *108*(B5), 2266, doi:10.1029/2002JB001946.

McCloskey, J., S. S. Nalbant, S. Steacy, C. Nostro, O. Scotti, and D. Baumont (2003), Structural constraints on the spatial distribution of aftershocks, *Geophys. Res. Lett.*, *30*(12), 1610, doi:10.1029/2003GL017225.

Nalbant, S. S., J. McCloskey, S. Steacy, and A. Barka (2002), Stress accumulation and increased seismic risk in eastern Turkey, *Earth Planet. Sci. Lett.*, *195*, 291–298.

Parsons, T., S. Toda, R. S. Stein, A. Barka, and J. H. Dieterich (2000), Heightened odds of large earthquakes near Istanbul: An interaction-based probability calculation, *Science*, *288*, 661–665.

Steacy, S., D. Marsan, S. S. Nalbant, and J. McCloskey (2004), Sensitivity of static stress calculations to the earthquake slip distribution, *J. Geophys. Res.*, *109*, B04303, doi:10.1029/2002JB002365.

Stein, R. S., G. C. P. King, and J. Lin (1992), Change in failure stress on the southern San Andreas fault system caused by the 1992 magnitude = 7. 4 Landers earthquake, *Science*, *258*, 1328–1332.

Stein, R. S., G. C. P. King, and J. Lin (1994), Stress triggering of the 1994 $M$ = 6.7 Northridge, California, earthquake by its predecessors, *Science*, *265*, 1432–1435.

Stein, R. S., A. A. Barka, and J. H. Dieterich (1997), Progressive failure on the North Anatolian fault since 1939 by earthquake stress triggering, *Geophys. J. Int.*, *128*, 594–604.

Toda, S., R. S. Stein, P. A. Reasenberg, J. H. Dieterich, and A. Yoshida (1998), Stress transferred by the 1995 $M_w$ = 6.9 Kobe, Japan, shock: Effect on aftershocks and future earthquake probabilities, *J. Geophys. Res.*, *103*, 24,543–24,565.

Wald, D. J., and T. H. Heaton (1994), Spatial and temporal distribution of slip for the 1992 Landers, California earthquake, *Bull. Seism. Soc. Am.*, *84*, 668–691.

Wald, D. J., T. H. Heaton, and D. V. Helmberger (1991), Rupture model of the 1989 Loma Prieta earthquake from the inversion of strong motion and broadband teleseismic data, *Bull. Seismol. Soc. Am.*, *81*, 1540–1572.

Wald, D. J., T. H. Heaton, and K. W. Hudnut (1996), The slip history of the 1994 Northridge, California, earthquake determined from strong ground motion, teleseismic, GPS, and leveling data, *Bull. Seismol. Soc. Am.*, *86*, S49–S70.

D. Baumont and O. Scotti, Institut de Radioprotection et de Sureté Nucléaire, BP 6 F-92265 Fontenay-aux-Roses, France.

J. McCloskey, S. S. Nalbant, and S. Steacy, School of Environmental Sciences, University of Ulster, Coleraine, BT52 1SA, Northern Ireland, UK. (s.steacy@ulster.ac.uk)

C. Nostro, Istituto Nazionale di Geofisica e Vulcanologia, Via di Vigna Murata, 605, 00143 Rome, Italy.